1 Appendix

1.1 Laminar Channel Flow

In laminar flow conditions, analytical solutions can be obtained for the pressure-driven, steady-state flow of Newtonian and power-law fluids in straight, rigid channels with constant cross section and no-slip boundary condition at the channel walls in some geometries. For the simple case of a Newtonian fluid in a circular channel with radius r, the dependence of the flowrate on the pressure drop along the channel is given by the Hagen-Poiseuille equation yielding a hydrodynamic resistance of $R = \Delta p/Q = \frac{8\eta L}{\pi r^4}$ for the channel. The corresponding flow profile is parabolic and the Newtonian wall shear-rate is given by $\dot{\gamma}_w = \frac{4Q}{\pi R^3}$. With an averaged diameter of $\tilde{h} = \sqrt{\pi} r$ the shape factor g (see eq. 4 in the main part of the manuscript) for the circular channel is thus given as $g = 4\sqrt{\pi}$. For power-law fluids in circular channels, the shape factor can be determined with the Weissenberg-Rabinowitsch equation[1] as

$$g(n) = \frac{(3n+1)\sqrt{\pi}}{n}. \tag{7}$$

For channels with rectangular constant cross sections $w \times h$, an analytical solution for the flow profile is only available for Newtonian fluids[2]. Moreover, in non-circular ducts, the shear rate is not constant along the wall. A semi-analytical solutions using average wall shearrates for the relation between flow rate and pressure $Q(p)$ for power-law fluids with $\eta(\dot{\gamma}) = A\dot{\gamma}^{n-1}$ in a duct with arbitrary constant cross section can be given as[3]:

$$Q = \frac{\lambda(n)\tilde{h}^{3+(1/n)}(\Delta p/L)^{1/n}}{A^{1/n}} \tag{8}$$

where the numerically determined shape factor $\lambda(n)$ is defined as $\lambda(n) \equiv \int_D \int \tilde{u} d\tilde{x} d\tilde{y}$ with the dimensionless coordinates $\tilde{x}, \tilde{y}, \tilde{u}$ of the cross section and the flow velocity in the channel direction. Thus, the shape factor λ depends on the power-law index n of the fluid and on the geometry of the duct. For some special geometries λ has been tabulated[3], and a method to calculate λ for rectangular ducts is available[4,5]. The corresponding averaged wall shear-rate can be calculated with eq. 4 in the main part, an expression for the shape dependence of $g(n)$ on the channel aspect ratio $\frac{h}{w}$ is given as[6]:

$$g\left(\tfrac{h}{w}, n\right) \equiv 4\left(\sqrt{\tfrac{h}{w}} + \sqrt{\tfrac{h}{w}}^{-1}\right)\left(b^\star\left(\tfrac{h}{w}\right) + \frac{a^\star\left(\tfrac{h}{w}\right)}{n}\right), \tag{9}$$

where $a^\star(x)$ ranges from $a^\star(0) = 0.5$ to $a^\star(1) = 0.2121$ and $b^\star(x)$ from $b^\star(0) = 1$ to $b^\star(1) = 0.6771$. The functions $a^\star, b^\star$ are tabulated in[6]. By combination of eqs. (8) and (9) we can determine the hydrodynamic resistance of the duct as

$$R = \frac{\Delta p}{Q} = \frac{\eta(\dot{\gamma}_w)L}{\tilde{h}^4 g^\star(\frac{h}{w}, n)} \tag{10}$$

with $g^\star(\frac{h}{w}, n) \equiv \lambda^n(n) g(\frac{h}{w}, n)^{n-1}$. For the evaluation of the experiments with rectangular channels of different aspect ratios used in this work, the shape factors $g(\frac{h}{w}, n)$ and $g^\star(\frac{h}{w}, n)$ have been calculated using FEM simulations of power-law fluid flows in rectangular channels. To this end, flow rate and averaged wall shear rate of the simulated flows have been determined in channels with aspect ratios from $\frac{h}{w} = 0.4$ to 1 with power-law exponents $n \in [0.2; 1]$. Fig. 5 shows contour plots of the evaluated shape factors $g^\star(\frac{h}{w}, n)$ and $g(\frac{h}{w}, n)$. Comparison of the numerical results for the Newtonian fluid ($n = 1$) with available analytical expressions[2] showed a numerical error smaller than 10% for all geometries under investigation.

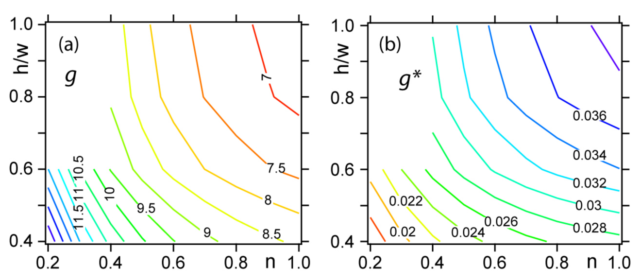

Figure 5: Shape factors $g(\frac{h}{w}, n)$ and $g^\star(\frac{h}{w}, n)$ in dependence of shear viscosity exponent n and channel aspect ratio h/w. $g(\frac{h}{w}, n)$ and $g^\star(\frac{h}{w}, n)$ have been evaluated for $n = 0.2, 0.3, \ldots, 1$ and $\frac{h}{w} = 0.4, 0.6, 0.8, 1$ from FEM simulations. For $n < 0.4$ and $\frac{h}{w} > 0.6$ the simulation did not converge.

1.2 Hencky strains at channel entrance of analyzer and reference channels K_a, K_r

For polymer solutions, the dependence of the entrance pressure drop Δp_{ent} on the elongational Hencky strain occuring at the channel entrance is strongly nonlinear and Δp_{ent} can be expected to be small $\Delta p_{\text{ent}} \approx 0$ for $\varepsilon < 1$[7]. The average elongational Hencky strain for fluid entering the analyzer and reference channel can be estimated with the ratio of the channel cross-sections D_f and $D_{a,r}$ of K_f and $K_{a,r}$: $\varepsilon_r = \ln(Q_r D_f/QD_r) = \ln(D_f/(X+1)D_r) \leq \ln(D_f/D_r)$; $\varepsilon_a = \ln(Q_a D_f/QD_r) = \ln(XD_f/(X+1)D_r) \leq \ln(D_f/D_r)$. In geometries A, B and D this yields $\varepsilon \leq 0.51$, so that the entrance pressure drop Δp^{ent} can be neglected. In geometry C the highest extensional strain occuring in the measurement is $\varepsilon \approx 2.6$. The extensional entrance pressure drop can be estimated as $\Delta p^{\text{ent}} = \Lambda(\dot{\varepsilon})\dot{\varepsilon}\varepsilon$.[8,9] Thus, the ratio of the entrance extensional pressure drop to the capillary pressure drop across the reference channel in geometry C can be estimated as $\frac{\Delta p^{\text{ent}}}{\delta p_r} \approx \frac{\Lambda(\dot{\varepsilon})}{\eta(\dot{\gamma})} \cdot 1.6 \cdot 10^{-5}$. Hence, even for high Trouton ratios $Tr = \Lambda(\dot{\varepsilon})/\eta(\dot{\gamma}) \sim 10^3 - 10^4$ the entrance pressure drop is insignificant for the measurement of $X(Q)$ in geometry C.

1.3 Validity of the approximation $Q_a/Q_r \approx d_a/d_r$

For a Newtonian fluid the flow profile in a rectangular channel with width w and height h, where $h < w$ is given by[2]

$$u_z(x,y) = \frac{4h^2 \mathrm{d}p/\mathrm{d}z}{pi^3 \eta} \sum_{n,\text{odd}}^{\infty} \frac{\sin(n\pi y/h)}{n^3} \left[1 - \frac{\cosh(n\pi x/h)}{\cosh(n\pi w/2h)}\right] \tag{11}$$

where $-0.5w < x < 0.5w$ and $0 < y < h$. For channels of high aspect ratio $h \ll w$ the lateral flow profile along the width of the channel is very flat, so that the flow is essentialy 2D. A numerical analysis shows, that $Q_{a,r} = \int_0^h \int_{-w/2}^{d_{a,r}} u_z(x,y)\mathrm{d}x\mathrm{d}y$ is well approximated by

$$Q_{a,r} = d_{a,r} \frac{h^3 w \mathrm{d}p/\mathrm{d}z}{12\eta} \left[1 - 0.630 \frac{h}{2d_{a,r} w}\right] \tag{12}$$

for $d_{a,r} > 2h$. Thus, the relative deviation δ_X of the width of the fluid streams $X_{\text{meas}} = d_a/d_r$ from the flow rate ratio $X = Q_a/Q_r$ is obtained as

$$\delta_X = 1 - \frac{d_a/d_r}{Q_a/Q_r} = \frac{0.63(1-2a)}{2w/h - 0.63(1-a)} \tag{13}$$

where $a = d_a/w$. Fig. 6 a shows δ_X in dependence of the aspect ratio h/w and ratio of the fluid stream widths X_{meas}. For non-Newtonian power-law fluids the flow profiles have to be numerically simulated to determine the error due to the approximation $Q_a/Q_r \approx d_a/d_r$. As this error is systematic, it is reduced by using the experimental value X_N^{exp} of the Newtonian flow ratio for the evalualuation of the power-law exponent: E.g. in a device with geometry A with a Newtonian flow rate ratio $X_{N,A} < 1$, the flow rate ratio for a power law fluid $X(Q) = X_N^{1/n}$ will also be smaller than unity. Thus, the experimental value $X_{N,A}^{exp}$ and $X(Q)^{exp}$ measured by d_a/d_R for Newtonian and power law fluids will both deviate from the real flow rate ratio into the same direction, so that the errors partially compensate. For the basic setup as in geometry A, the remaining deviation in n caused by the approximation is calculated as

$$\frac{n_{\text{meas}}}{n} = \frac{\ln X_N^{\text{meas}}}{\ln X^{\text{meas}}} \frac{\ln X}{\ln X_N}, \tag{14}$$

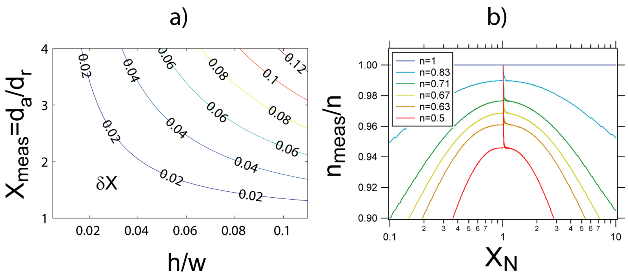

Figure 6: (a) Relative error of the flow ratio δ_X caused by the approximation $X = Q_q/Q_r \approx d_a/d_r$ in dependence of the channel aspect ratio h/w and ratio of the fluid stream widths $X_{\text{meas}} = d_a/d_r$ calculated for the flow profile of a Newtonian fluid. (b) The resulting error in the power-law index n for geometry A is shown by the ratio between the measured power-law index n_{meas} and the real value n for values of $n = 1.0, 0.83, 0.71, 0.67, 0.63, 0.5$. The underlying non-Newtonian flow profiles where calculated numerically. The error can be kept smaller by chosing a geometry, where X_N is close to unity (e.g. geometry B).

where X and X_N are related by eq. (6) in the main paper as $X = X_N^{1/n}$. Figure 6b shows the ratio of the power-law index determined by d_a/d_r to the exact value for several values of n in dependence of the Newtonian value X_N of the device. By designing devices with moderate values for the Newtonian flow ratio with $X_N \in [0.5; 2]$ the error is kept small ($\leq 7\%$). In principle, this systematic error could be accounted for in the numerical evaluation of the measurements.

1.4 Experimental error

Repeated measurements with Newtonian glycerol solutions showed that the experimental error in determining the flow rate ratio $X(Q)^{exp} = d_a/d_R$ is on the order of 1%. However, the measured values $X(Q)^{exp}$ for the 1% PAA and 2% PAA polymer solutions suggest a bigger error of about 5% (e.g. see fig. 3a in main section). Stronger deviations might occur due to temporal dirt or undiscovered air bubbles changing the channels resistance or degradation of the polymer solution. Thus, an errorbar of $\pm 5\%$ was used for the values in fig. 3a. The overall resulting error for the evaluation of $n(\dot{\gamma})$ can be estimated from the 2% PAA measurement data (red symbols) from different geometries in fig. 4. The standard relative deviation from the polynomial fit curve (red solid line) is 6%. This value was taken as the errorbar for $n(\dot{\gamma})$ of both the 1% and 2% PAA solutions.

1.5 Numerical evaluation of shear exponent $n(\dot{\gamma})$

By simultaneously using N measured values of the flow ratio $X(Q)$ on an interval $[Q_{\min}; Q_{\max}]$ it is possible to numerically determine $j = 1 \ldots N$ interpolation values H_j^S for the shear viscosity on the interval of shear rates $[\dot{\gamma}_{\min}; \dot{\gamma}_{\max}]$ associated with $[Q_{\min}; Q_{\max}]$. Instead of assuming a power-law, the method is based on a linear interpolation for the logarithmized values of the viscosity between the N values H_j^S. Then, eq. 2 in the main partleads to a linear equation system for the N unknown viscosity values H_j^S. Due to the differential nature of the measurement, the viscosity curve given by H_j^S is indefinite in its absolute value, yet the shape of the viscosity curve and the corresponding values for the viscosity exponent $n(\dot{\gamma})$ are fixed. As the viscosity must be monotonic on each of the interpolated intervals $[\dot{\gamma}_j, \dot{\gamma}_{j+1}]$ once the width of the shear rate intervals $(\dot{\gamma}_{\min} - \dot{\gamma}_{\max})/(N-1)$ is sufficiently small, the method gives much more accurate values than the direct evaluation with eq. 6 (main part). With the $p(Q)$-curve for the pressure drop across the channels K_a, K_r being monotonically increasing with the flow rate, the roughness of $X(Q)$ is physically limited, so that strong fluctuations in $X(Q)$ have to be attributed to experimental error. Therefore, with a sufficient density of measurement values on $[Q_{\min}; Q_{\max}]$, the N measurement values $X_j(Q)$ can be fitted with a smoothing function without losing information on the viscosity curve. The solid dark blue line in fig. 3b in the main part shows a polynomial fit of order 7 to the measured $X(Q)$ values of the WLM-solution, the resulting curves for the viscosity exponent $n(\dot{\gamma})$ and the integrated viscosity $\eta(\dot{\gamma})$ are shown by the dashed blue lines in fig. 4 (main part).

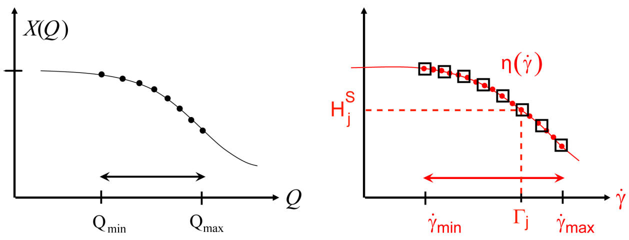

Figure 7: Schematics of the numerical evaluation method: The N measurement values of X on $[Q_{\min}, Q_{\max}]$ (●, left) correspond to $2N$ unknown viscosity values at $2N$ shear-rates on $[\dot{\gamma}_{\min}; \dot{\gamma}_{\max}]$ (red ●, right). The $2N$ viscosity values are apporoximated by interpolation between N viscosity values (□), for which a linear equation system containing the N measured values for X can be solved.

In detail, for the numerical evaluation, N interpolation points Γ_j were distributed over the interval $[\dot{\gamma}_{\min}, \dot{\gamma}_{\max}]$

$$\Gamma_j = \dot{\gamma}_{\min} \cdot \left(\frac{\dot{\gamma}_{\max}}{\dot{\gamma}_{\min}} \right)^{j/(N-1)} \tag{15}$$

where the according interpolation values for the viscosity were set:

$$H_j^S \equiv \eta(\Gamma_j) \tag{16}$$

The $2N$ unknown values $\eta(\dot{\gamma}_{a,i}), \eta(\dot{\gamma}_{r,i})$ corresponding to the N measurement points $X_i(Q)$ on the interval

$[Q_{\min}; Q_{\max}]$ can thus be expressed by the N unknown interpolation values H_j^S using the interpolation hat function

$$F_h(x) = \begin{cases} 0 & \text{for} \quad x < -1 \\ x+1 & \text{for} \quad -1 \leq x \leq 0 \\ 1-x & \text{for} \quad 0 < x \leq 1 \\ 0 & \text{for} \quad x > 1 \end{cases} \tag{17}$$

as

$$\eta(\dot{\gamma}_{k,i}) = \sum_j N_{k,ij}^S(\dot{\gamma}_{k,i}) H_j^S, \quad \text{with} \quad N_{k,ij}^S(\dot{\gamma}_{k,i}) = F_h(x_{k,ij}^S(\dot{\gamma}_{k,i})) \tag{18}$$

where $k = a, r$ and

$$x_{k,ij}^S(\dot{\gamma}_{k,i}) = (N-1)\frac{\log \dot{\gamma}_{k,i} - \log \dot{\gamma}_{\min}}{\log \dot{\gamma}_{\max} - \log \dot{\gamma}_{\min}} - j + 1 \tag{19}$$

Using eq. (18) we can rewrite eq. 2 from the main paper as:

$$(X_i L_a \sum_j N_{a,ij}^S H_j^S - L_r \sum_j N_{r,ij}^S H_j^S) = 0. \tag{20}$$

This is a linear, homogeneous equation system with N equations, which can be written with the vector $\mathbf{H} = (H_1^S, \ldots, H_N^S)^T$ as:

$$\mathbf{M}^S \cdot \mathbf{H} = 0, \tag{21}$$

where

$$M_{i,j}^S = X_i L_a N_{a,ij}^S - L_r N_{r,ij}^S, \quad i, j = 1, \ldots, N \tag{22}$$

Eq. 21 does not define a unique solution for the viscosity, and any multiple $\mathbf{H}' = a\mathbf{H}$ of a solution $\mathbf{H}$ is a solution too. To obtain absolute values of the viscosity, one value of $\eta(\dot{\gamma})$ on the interval has to be known. However, the local powerlaw exponents which can be obtained by differentiating the numerical solution given by $\mathbf{H}$ are uniquely defined. For the numerical solution for the WLM-solution measurement, the discretized polynomial fit to the measurement points shown in fig. 3a (solid blue line) was used for the input data $X_i(Q)$ instead of the real measurement points. The resulting viscosity curve $\eta(\dot{\gamma}$ is shown in the inset of fig. 4b (main paper, dashed blue line), the values for $n(\dot{\gamma}$ (solid blue line fig. 4) were determined by differentiation.

The numerical method reproduces the low values of $n \approx 0$ observed for high shear rates with the rotational rheometer, and the shape of the viscosity curve $\eta(\dot{\gamma})$ from the differential measurement is in excellent agreement with the cone-plate rheometer values (dashed blue line and blue squares in the inset of fig. 4, main section).

References

[1] C. W. Macosco, *Rheology. Principles, Measurements and Applications*, John Wiley & Sons, 1994.

[2] Henrik Bruus, *Theoretical Microfluidics*, Oxford University Press, 2007.

[3] T. Liu, *Fully developed flow of power-law fluids in ducts*, Ind. Eng. Chem. Fundam. **22** (1983), 183–186.

[4] S. Middleman, *Flow of power law fluids in rectangular ducts*, Trans. Soc. Rheol. **9** (1965).

[5] R. S. Schechter, *On the steady flow of a non-Newtonian fluid in cylinder ducts*, AIChE Journal **7** (1961), 445–448.

[6] Y. Son, *Determination of shear viscosity and shear rate from pressure drop and flow rate relationship in a rectangular channel*, Polymer **48** (2006), 632–637.

[7] S. L. Anna and G. H. McKinley, *Elasto-capillary thinning and breakup of model elastic liquids*, Journal of Rheology **45** (2001), 115–138.

[8] F. N. Cogswell, *Converging flow and stretching flow - compilation*, Journal of Non-Newtonian Fluid Mechanics **4** (1978), 23–38.

[9] A. G. Gibson, *Converging dies, in "Rheological Measurement" by A. A. Collier amd D. W. Clegg*, 2nd ed., Elsevier Applied Science, London, 1988.